SCIENCE CHINA
Earth Sciences

• RESEARCH PAPER •

March 2017 Vol.60 No.3: 589–601
doi: 10.1007/s11430-016-5069-4

Lithospheric structure and faulting characteristics of the Helan Mountains and Yinchuan Basin: Results of deep seismic reflection profiling

LIU BaoJin*, FENG ShaoYing, JI JiFa, WANG ShuaiJun, ZHANG JianShi, YUAN HongKe & YANG GuoJun

Geophysical Exploration Center of China Earthquake Administration, Zhengzhou 450002, China

Received July 28, 2016; accepted October 20, 2016; published online January 4, 2017

Abstract The Helan Mountains and Yinchuan Basin (HM-YB) are located at the northern end of the North-South tectonic belt, and form an intraplate tectonic deformation zone in the western margin of the North China Craton (NCC). The HM-YB has a complicated history of formation and evolution, and is tectonically active at the present day. It has played a dominant role in the complex geological structure and modern earthquake activities of the region. A 135-km-long deep seismic reflection profile across the HM-YB was acquired in early 2014, which provides detailed information of the lithospheric structure and faulting characteristics from near-surface to various depths in the region. The results show that the Moho gradually deepens from east to west in the depth range of 40–48 km along the profile. Significant differences are present in the crustal structure of different tectonic units, including in the distribution of seismic velocities, depths of intra-crustal discontinuities and undulation pattern of the Moho. The deep seismic reflection profile further reveals distinct structural characteristics on the opposite sides of the Helan Mountains. To the east, The Yellow River fault, the eastern piedmont fault of the Helan Mountains, as well as multiple buried faults within the Yinchuan Basin are all normal faults and still active since the Quaternary. These faults have controlled the Cenozoic sedimentation of the basin, and display a "negative-flower" structure in the profile. To the west, the Bayanhaote fault and the western piedmont fault of the Helan Mountains are east-dipping thrust faults, which caused folding, thrusting, and structural deformation in the Mesozoic stratum of the Helan Mountains uplift zone. A deep-penetrating fault is identified in the western side of the Yinchuan Basin. It has a steep inclination cutting through the middle-lower crust and the Moho, and may be connected to the two groups of faults in the upper crust. This set of deep and shallow fault system consists of both strike-slip, thrust, and normal faults formed over different eras, and provides the key tectonic conditions for the basin-mountains coupling, crustal deformation and crust-mantle interactions in the region. The other important phenomenon revealed from the results of deep seismic reflection profiling is the presence of a strong upper mantle reflection (UMR) at a depth of 82–92 km beneath the HM-YB, indicating the existence of a rapid velocity variation or a velocity discontinuity in that depth range. This is possibly a sign of vertical structural inhomogeneity in the upper mantle of the region. The seismic results presented here provide new clues and observational bases for further study of the deep structure, structural differences among various blocks and the tectonic relationship between deep and shallow processes in the western NCC.

Keywords North China Craton, Deep seismic reflection profile, Lithospheric structure, Helan Mountains, Yinchuan Basin

Citation: Liu B J, Feng S Y, Ji J F, Wang S J, Zhang J S, Yuan H K, Yang G J. 2017. Lithospheric structure and faulting characteristics of the Helan Mountains and Yinchuan Basin: Results of deep seismic reflection profiling. Science China Earth Sciences, 60: 589–601, doi: 10.1007/s11430-016-5069-4

* Corresponding author (email: lbj001@126.com)

1. Introduction

The North China Craton (NCC), formed in the Archean Eon, is one of the world's oldest cratons. It distinguishes itself from other cratons in the world by its remarkable lithospheric thinning and the property changes in the eastern NCC (Carlson et al., 2005). Recent studies on the NCC and its adjacent areas showed that the NCC's destruction, alteration, and lithospheric thinning are spatially inhomogeneous. The eastern NCC has undergone intense alteration and destruction from the Late Mesozoic to the Cenozoic era, accompanied by a wide range of magmatic activities, including large-scale tectonic extensions and faulted basin. The lithospheric thickness increases gradually westward from 60–80 km near the Tan-Lu fault zone to ~90 km at the piedmont of the Taihang Mountains (Ren et al., 2002; Chen et al., 2008; Deng et al., 2006; Zhu et al., 2008; Tian et al., 2009; Zheng and Wu, 2009; Zhu et al., 2011; Guo et al., 2012; Wu et al., 2014). In the middle NCC, the lithospheric thickness is significantly different on both sides of the nearly SN-trending Taihang Mountains gravity gradient zone, which increases gradually from 80–90 km on the North China Plain to >120 km in the western Taihang Mountains. This may represent a type of transitional craton (Xu, 2007; Li et al., 2011; Zhu et al., 2012; Wang et al., 2014; Liu et al., 2015; Duan et al., 2015). In contrast to the tectonic characteristics of the eastern NCC, the western NCC lacks large-scale regional tectonic extensions. Extensional deformation has been localized in two elongated narrow circum-Ordos rift zones since the Cenozoic era (i.e., the Yinchuan-Hetao and Shaanxi-Shanxi rift zones) (Deng et al., 1999; Zhang et al., 2003). Recent studies have found that the lithospheric thickness of the western NCC exhibits strong lateral inhomogeneity, i.e., the lithospheric thickness under the Ordos Basin is ~200 km, whereas under the Yinchuan-Hetao and Shaanxi-Shanxi rift zones, it is less than 100 km (Chen et al., 2009, 2010; Zhu et al., 2011; Zhang et al., 2009).

As a tectonic boundary zone in the western NCC, the Helan Mountains and Yinchuan Basin (HM-YB) is both an intracontinental tectonic deformation zone and a complex active tectonic zone that has undergone long-term tectonic evolution (Deng et al., 1999). The geophysical evidence is still insufficient to resolve the scientific uncertainties related to its deep structure, notably: What are the deep structural differences between the HM-YB active tectonic zone and the stable Ordos block? What are the tectonic combinational patterns within the HM-YB region? How do deep processes affect the shallow structure? To address these issues, a high-resolution deep seismic prospecting method was used to image the fine lithospheric structure of the HM-YB. The aim is to achieve an in-depth understanding of the structural differences between the tectonic boundary zone in the western NCC and its adjacent blocks, as well as their impact on lithospheric structure and tectonic evolution. This would help us to gain comprehensive knowledge of the complex geological characteristics in the present-day NCC, as well as provide critical constraints on the spatial heterogeneity and dynamic processes of the NCC destruction. In early 2014, we carried out a 135-km-long deep seismic reflection profiling and a 500-km-long wide-angle reflection/refraction profiling in the western NCC. This work was supported by the "Major Research Plan of National Natural Science Foundation of China: NCC destruction". In this paper, we apply data from the deep seismic reflection profile, in a combination with partial data from the wide-angle reflection/refraction profile (complete wide-angle reflection/refraction profile findings will be discussed in a separate paper), to discuss and analyze the fine deep-shallow structure in the HM-YB region and the characteristics of the faults. The results also provide seismological evidence for research on the structural differences between the HM-YB and its adjacent blocks, the deep processes, and the relationship between deep and shallow tectonics.

2. Geological structure overview and seismic profile location

In geotectonic terms, the HM-YB is located at the northern end of the North-South tectonic Zone (Figure 1). The main tectonic deformations in this region since the Cenozoic are intracontinental extensional deformations. The region also shows evidence of strike-slip extensional tectonic deformation similar to those in North China (Xu et al., 1993; Deng et al., 1999). The HM-YB extend in a NNE direction, with the stable Alashan block and Ordos block to the west and east, respectively, and the southern edge is connected to the arcuate structural zone of the Qinghai-Tibet Plateau's northeastern margin. The topography of the Helan Mountains is as follows: it slopes steeply eastward and gently westward, and is much wider in the north and narrower in the south. The highest peak of the Helan Mountains is 3556 m, which is 2200 m higher than the Yinchuan Basin. The Yinchuan Basin is a Cenozoic rifted basin, and its eastern and western boundaries are controlled by the eastern piedmont fault of the Helan Mountains and the Yellow River fault, respectively. The thickness of the Cenozoic sediment within the basin is ~7000 m, with the Quaternary layer reaching to a maximum thickness of 1200–1400 m (Tang et al., 1992; SSB, 1988; Chai et al., 2011).

The HM-YB is located in the area where the Alashan and Ordos blocks connect. The region was an aulacogen from the Neoproterozoic to Early Paleozoic eras, with rifting occurring during the Late Paleozoic and a collision valley from the mid-Mesozoic. NW-SE compressive stress during the Late Mesozoic led to NNE folding and extrusion thrusting faults; consequently, the Mesozoic stratum underwent folding and thrusting, and the Helan Mountains began to be folded and uplifted. An intracontinental extensional phase occurred

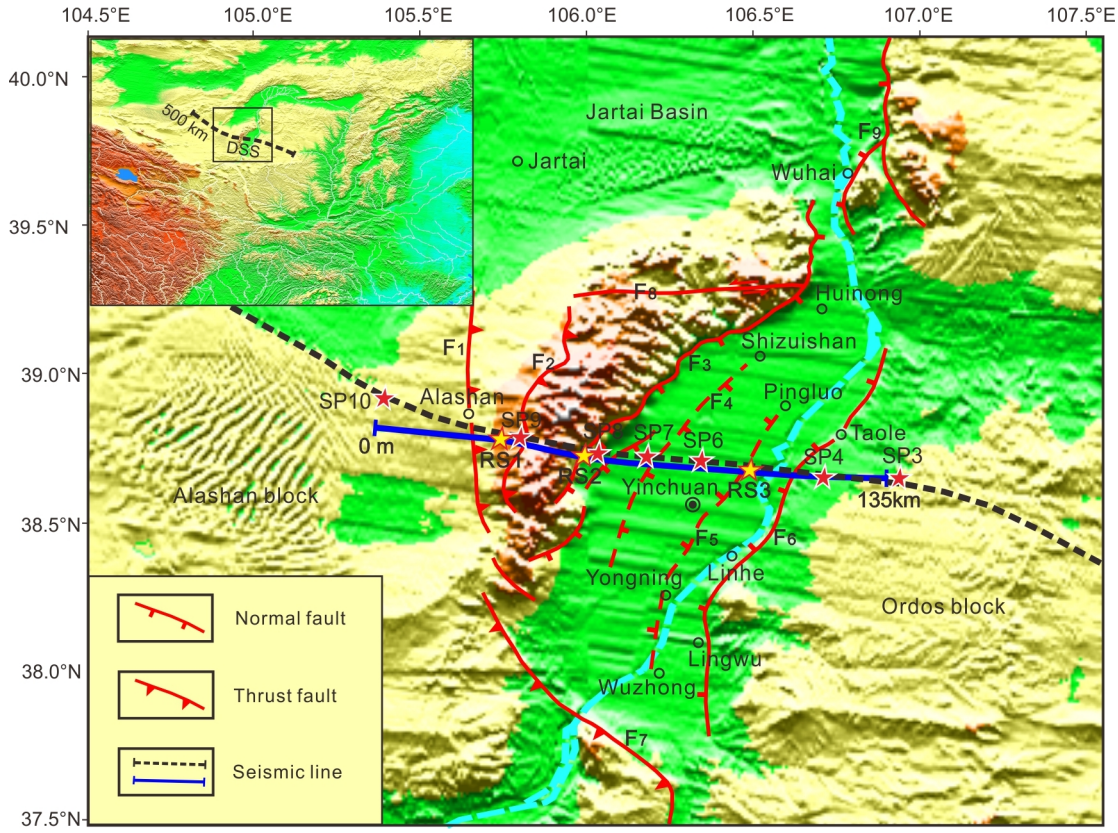

Figure 1 Geological structure and location of deep seismic reflection profile in the research region. F1: Bayanhaote fault; F2: western piedmont fault of Helan Mountains; F3: eastern piedmont fault of Helan Mountains; F4: Luhuatai fault; F5: Yinchuan fault; F6: Yellow River fault; F7: Qingtongxia-Guyuan fault; F8: Zhengyi Guan fault; F9: frontal fault of Table Mountains; blue solid line indicates deep seismic reflection profile; black dotted line is wide-angle reflection/refraction profile; yellow stars correspond to shot-points of deep seismic reflection profile shown in Figure 2; red stars correspond to shot-points of wide-angle reflection/refraction profile shown in Figure 3.

from the Eocene to the Oligocene, and it triggered the development of the Yinchuan Graben. The main period of extensional tectonic deformation in the HM-YB was the Late Cenozoic, and the process continues today (SSB, 1988; Zhang et al., 1998; Darby and Ritts, 2002; Zhang et al., 2008). Studies of the apatite fission track age of the Helan Mountains and the sedimentation rate of the Yinchuan Basin's stratum (Zhao et al., 2007; Liu et al., 2010) suggested that the effects of the NW-SE extension caused large-scale uplift of the Helan Mountains during the Eocene and fast-paced uplift of the Helan Mountains since the Pliocene. During the same periods, the Yinchuan Basin, a Cenozoic basin formed concurrently with the Helan Mountains, underwent intense sedimentation.

The faults of the HM-YB is well developed. East of the Helan Mountains, an active normal fault (i.e., the eastern piedmont fault of the Helan Mountains) connects to the Yinchuan Basin. Active thrust faults (i.e., the Bayanhaote fault and the western piedmont fault of the Helan Mountains) have developed in the western section of the Helan Mountains. The Zhengyiguan strike-slip fault is in the north of the Helan Mountains, and it was reactivated during the Cenozoic era (Figure 1). The eastern boundary of the Yinchuan Basin is the west-dipping Yellow River normal fault. The east-dipping Luhuatai buried active fault and west-dipping Yinchuan buried active fault developed in this basin (Yan and Wang, 2002; Liu et al., 2010; Chai et al., 2011; Lei et al., 2014).

The nearly EW-trending, 135-km-long deep seismic reflection profile traverses the major faults in the research region (Figure 1). The profile starts at the intersection between the Gobi and the desert southwest of the Alashan Left Banner in Inner Mongolia (38°46′52.8″N, 105°22′32.5″E). Going eastward, the profile traverses the Helan Mountains and Yinchuan Basin, and ends at the Taoligacha village on the western margin of the Ordos block (38°36′59.3″N, 106°51′27.5″E). The near-surface geological conditions along the deep seismic reflection profile are complex and changeable. To the west of Profile Distance ~23 km, there is a piedmont alluvial zone and the Gobi desert, with an uncompacted mixture of sand and gravel on the surface and deep phreatic water level. Between Profile Distance 23 and 56 km is the Helan Mountains, with a highly undulating terrain, and the Mesozoic and Paleozoic bedrocks in this section directly outcrop on the ground surface, resulting in tremendous challenges for transportation and fieldwork. The Yinchuan Basin is located between Profile Distances 56 and 110 km, and has a relatively flatter ter-

rain. In this section, the Cenozoic sedimentary layer within the basin is thick, and the near-surface structure consists of loosely structured Quaternary sediments; in addition, towns and villages are in a dense distribution, and roads crisscross one another to form a complex network. Those conditions result in strong external interferences. To the east of Profile Distance 110 km is the Ordos block, and its ground surface is mostly covered by aeolian sand dunes and the phreatic surface is deep, which is not conducive to the excitation and reception of seismic waves. Targeted technical measures have to be adopted for field surveying to circumvent above-mentioned obstacles and to acquire high-quality deep seismic reflection data.

3. Seismic data acquisition and process

3.1 Data acquisition

The target probing layer for this study was deep. In addition, consideration was given to imaging shallow structures and other characteristics such as the near-surface complex geological environment of the study area. Deep seismic reflection data were acquired using spread geometry with 45 m station spacing, 45 m offset, 450 m shot spacing, 1200 recording channels, and 60-folds of common mid-point (CMP). Such spread geometry was not only conducive to imaging complex interfaces, but was also effective in capturing reflection data from the shallow layer. For the deep target layer, the spread geometry was also able to maintain an adequate normal moveout of the reflection phase, thereby improving the accuracy with which the velocities of the interface's reflection were acquired (Yilmaz, 1994; Sheriff and Gardner, 1999). When first-arrival wave imaging technologies were applied, first-arrival wave data from the common-shot gathers were also used to obtain the velocity structure of the basement along the profile. The latter in turn allowed us to study and analyze the stratum structure and tectonics of the upper crust.

Seismic wave excitation is the prerequisite for acquiring seismic data with high signal-to-noise ratios. Considering the deeper target probing layer, we applied a longer seismic spread. In order to obtain high-resolution seismic reflection images of the entire lithosphere, we used two types of explosion sources with shot charges of 48 kg and 300 kg, respectively, during our seismic survey. The 48 kg shots were performed in every 450 m interval. The 300 kg shots were executed every 1800 m. This spread geometry for the 48 kg and 300 kg shot sources provided 60-fold common mid-point (CMP) coverage for the processing. The seismic wave excitation and data acquisition parameters are shown in Table 1.

The common-shot gathers at the different tectonic sections along the profile are shown in Figure 2 (refer to RS1–RS3 of Figure 1 for shot-point location). To analyze and compare the characteristics of reflection events from various depths more accurately, we conducted time-varying band-pass filtering and linear interference suppression for raw common-shot gathers. Several sets of clear reflection phases from the crust and upper mantle are present in the common-shot gathers, and the characteristics of the seismic wavefield are different among the various tectonic sections (Figure 2). Seismic records from the RS1 shot-point located in the western Helan Mountains (Figure 2a) indicate an abundance of crustal reflection phases. Strong CR_1-CR_2 reflections with good horizontal continuity are detected within the crust, and there is a series of weaker reflection events with complex, varying properties and definite extensional lengths, which indicate that the crustal reflection structure beneath the Helan Mountains is complicated. Below the Helan Mountains, both the Moho reflection and upper mantle reflection (UMR) are west-dipping, and their two-way travel times (TWT) are 15–16 s and 22–24 s, respectively. The seismic records of the RS2 shot-point located at the meeting point of the Helan Mountains and the Yinchuan Basin (Figure 2b) reveal various sets of intra-crustal reflections with strong reflection energy beneath the Helan Mountains; however, the strong reflection phases within the middle–lower crusts of the Yinchuan Basin are missing, which indicates that the constitution of crustal matter in the Helan Mountains and Yinchuan Basin might differ. The strong Moho reflections exhibit lateral discontinuities on the eastern side of the Helan Mountains, and the arrival times of the Moho reflections from the two sides of the discontinuity zone are different. The UMRs in this sec-

Table 1 Parameters for data acquisition of deep seismic reflection profile

Contents	Main parameters
Seismic survey line	Length of survey line: 135 km; Number of shots: 301; Number of Stations: 3001
Seismic source	Dynamite: 48 kg; Shot hole depth: 30 m; Source spacing: 450 m Dynamite: 300 kg; Shot hole depth: 50 m; Source spacing: 1800 m
Seismic receiver	Geophone Frequency: 10 Hz (12/string, point combination) Geophone group spacing: 45 m; Channels: 1200 active; CMP-fold: 60 Minimum offset: 45 m; Maximum offset: 49455 m Spread geometry: 27055 m-45 m-45 m-45 m-27055 m
Seismic instrument	428XL seismometer; Sampling rate: 4 ms; Recording length: 30 s

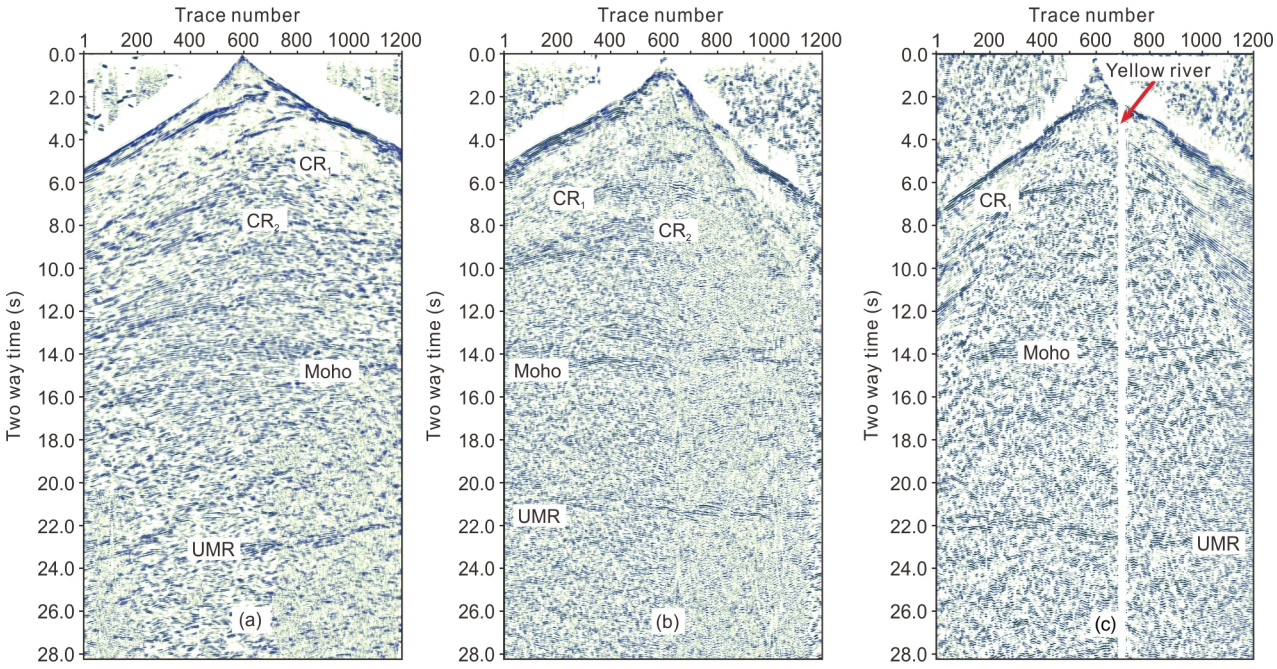

Figure 2 Common-shot point gathers of deep seismic reflection profile.

tion have a good lateral continuity and a slightly east-dipping attitude. Figure 2c shows the seismic records of the RS3 shot point located at the junction of the Yinchuan Basin and the Ordos block. There are practically no reflection groups with relatively lateral continuity in the middle-lower crusts between the Moho and reflection interface CR_1. The travel time of Moho reflections in this section is TWT ~14 s and their attitudes are nearly horizontal. The UMRs are reliably identified on both the eastern and western sides of the Yellow River, and their interfaces dip eastward.

3.2 Seismic data processing and the profile's velocity structure

The deep seismic reflection data were processed using the conventional CMP method. The raw common-shot gathers were characterized by strong linear interferences and large differences in frequency and energy from the deep-shallow reflector, as well as high levels of static correction caused by elevation differences in the terrain. Hence, interference suppression, improving signal-to-noise ratios, and proper static corrections were the priorities during data processing. The main methods and parameters for data processing are shown in Table 2. The former include geometric diffusion correction, surface-consistent amplitude compensation, linear interference suppression, tomographic static correction, time-variant bandpass filtering, 2D filtering, surface consistent deconvolution, velocity analysis, dynamic correction, multi-iterative residual static correction, dip moveout (DMO) correction, and post-stack denoising.

To obtain the velocity structure at different depths along the profile, we applied a first-break wave imaging method based on nonlinear refraction travel-time tomography using first-break wave information from common-shot gathers (Zhang and Toksöz, 1998) to obtain the basement velocity structure (Figure 3a). Next, we conducted tomographic static correction of the deep seismic reflection data and analysis of the basement's structure. The crustal 2D velocity structure of the deep seismic wide-angle reflection/refraction profile was applied to determine the velocity of seismic waves under the basement. Figure 3b shows the crustal 2D velocity structural model and crustal layering results for the overlapping sections of the deep seismic reflection profile. The crustal structure of this region is a three-layer model with an upper, middle, and lower crust. The crustal thickness along the profiles is 40–48 km. The Moho gradually deepens from east to west, with significant uplifts beneath the Yinchuan Basin, and depressions beneath the Helan Mountains, which correspond to a "mirror image" of the basement. The crustal P-wave velocities show different distribution characteristics between the two sides of the Yinchuan Basin. Within the Ordos block, the positive gradient for crustal P-wave velocities increases with depth, without the low-velocity layer (LVL) in the crust. In contrast, low-velocity anomalies are seen in the middle-lower crust beneath the Helan Mountains. This difference illustrates the region's structural complexity. To obtain the depth of UMRs during data processing and interpretation, we referred to the lithospheric 2D P-wave velocity data from the Wendeng-Alashan Left Banner seismic wide-angle reflection/refraction profile (Wang et al., 2014).

Table 2 Processing methods and parameters for deep seismic reflection data

Main contents	Processing method	Processing parameter
Data decompilation and records editing	Manual editing	Applied
Amplitude compensation	Correction of spherical diffusion	1.2 (Exponent)
	Automatic gain control (AGC)	1500 ms
	surface consistent Amplitude compensation	Applied
Noise suppression	Time-variant bandpass filtering	0–6 s (15–65 Hz); 6–15 s (10–55 Hz); 15–30 s (8–45 Hz)
	Automatic recognition and elimination of linear interferences	±2000 m s^{-1}
Deconvolution	Surface consistent deconvolution	Predicted length: 30 ms; Window length: 2000 ms; Operator length: 120 ms; White noise coefficient: 0.15
Static correction	Tomographic static correction	Applied
	Residual static correction	Maximum temporal shift: 16 ms
Velocity analysis	Velocity spectrum	0–8 s; Distance interval: 1125 m
	Constant-speed scanning	8–30 s; Velocity interval: 200 m s^{-1}
Dynamic correction and stacking	NMO stretch muting	Manual mute
	CMP root mean square stacking	CMP interval: 22.5 m, 60-fold
DMO correction	Common offset of DMO	Inclination: 60°; Aperture width: 4500 m
Post-stack processing	F-X predictive filtering	Number of lateral traces: 151; Temporal window: 300 ms
	Balancing energy of stacked traces	AGC window: 1000 ms

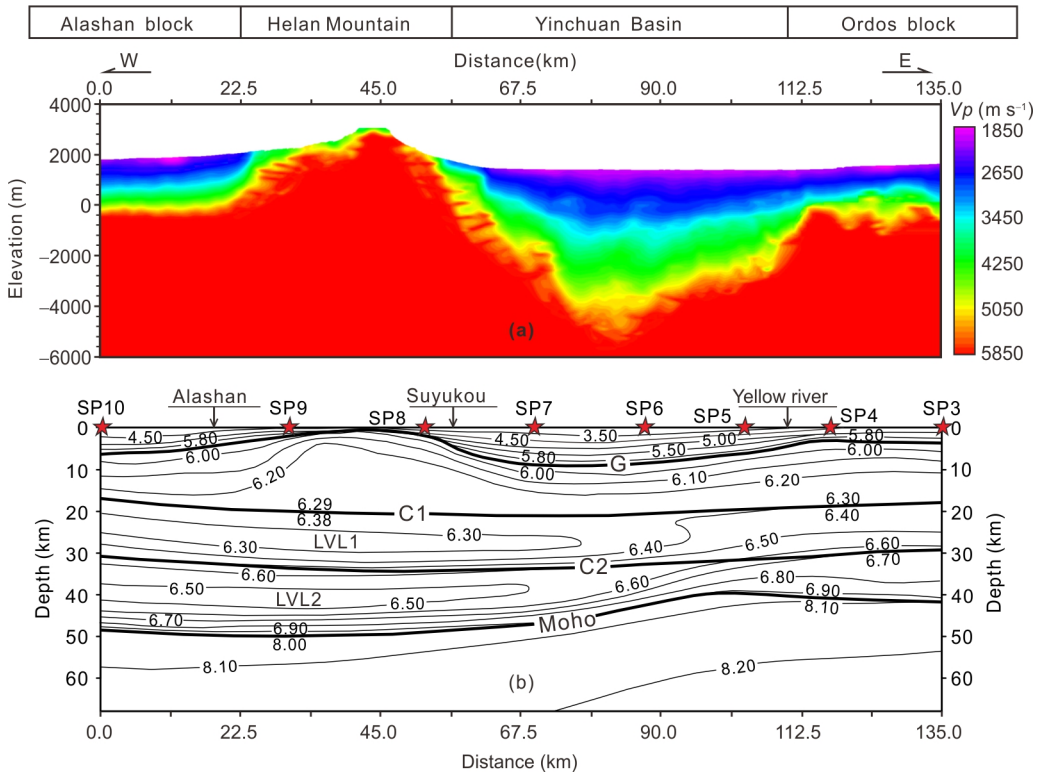

Figure 3 Basement velocity structure (a) and crustal 2D velocity structure (b).

4. Reflection structure characteristics of the deep seismic reflection profile

From west to east, the deep seismic reflection profile traverses the eastern margin of the Alashan block, Helan Mountains, Yinchuan Basin, and western margin of the Ordos block. The stacked time section of deep seismic reflection and geological structure along the profile are shown in Figure 4. The deep

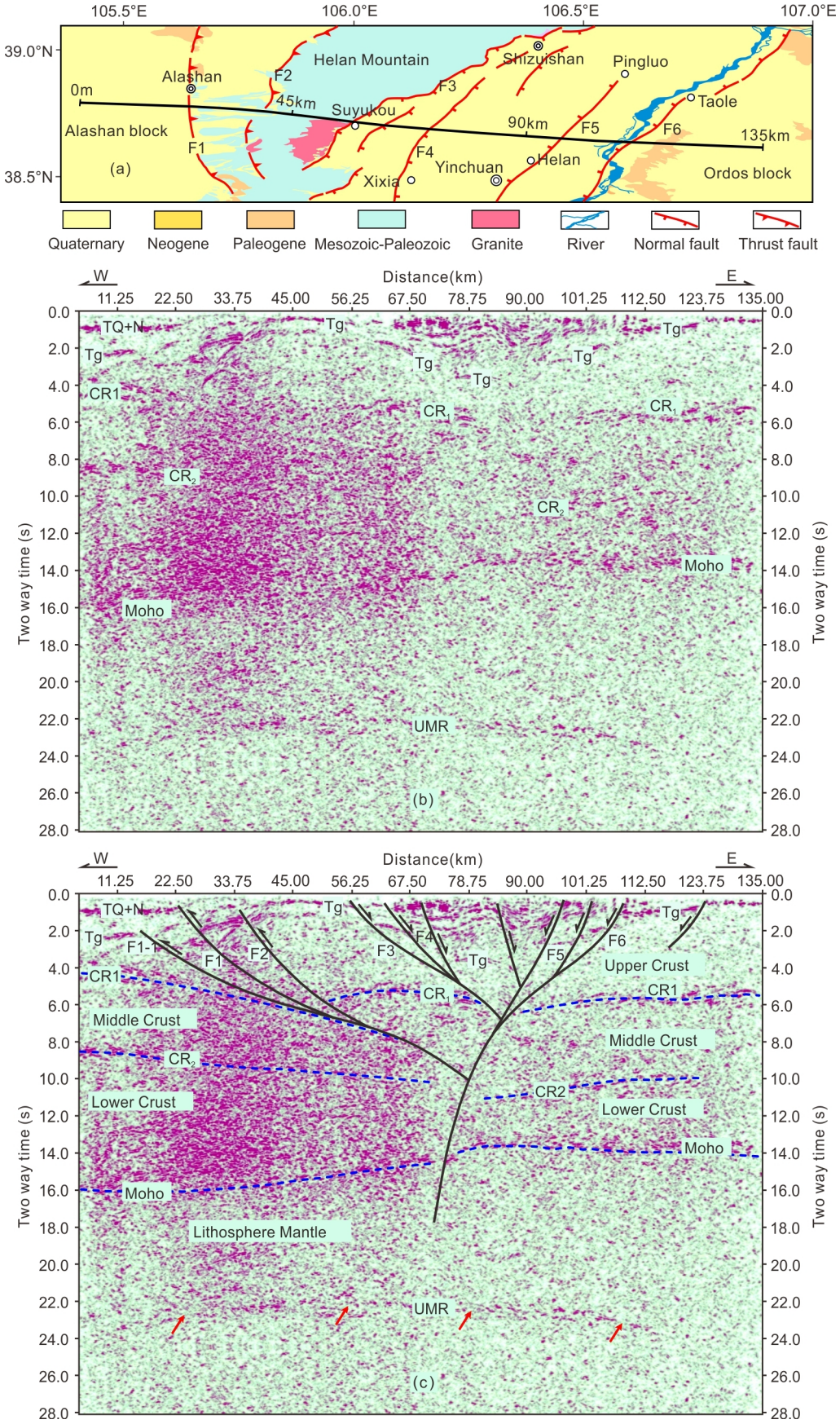

Figure 4 Geological structure (a), stacked time section of deep seismic reflection (b) and interpretation of deep seismic reflection profile (c).

seismic reflection profile (Figure 4b) shows clear images of the crustal structure and tectonics. In the transverse direction, the deep seismic reflection profile is bounded by the Helan Mountains in the east, and there are significantly different characteristics of reflection structures on its east and west sides. In the vertical direction, the Moho's strong reflection acts as a longitudinal boundary, dividing the profile into a crust with obvious reflective properties and the lithospheric mantle with weak reflection. The reflection structure characteristics of the profile are summarized as follows.

4.1 Reflection structure characteristics of the upper crust

The staked time section (Figure 4) shows that the upper crustal structure of the region is characterized by an uplift-and-depression distribution, with different tectonic positions having different reflection structures. On the eastern edge of the Alashan block (i.e., west of Profile Distance ~22 km), the basement reflector Tg and the bottom boundary reflector of the Neogene (T_{N+Q}) have a nearly horizontal distribution with a good lateral continuity, which shows sedimentary layer reflector characteristics. The TWT of reflectors T_{N+Q} and Tg are ~800 ms and ~2200 ms, respectively, with corresponding buried interface depths of 800–900 m and 2400–2500 m, respectively. West of the Helan Mountains (i.e., between Profile Distance 23 and 45 km), the upper crustal reflection is formed by several lateral, discontinuous, and west-dipping strong reflections. The dip angle of the stratum's reflection surface increases gradually with depth, and fold morphology is clear, with thrust structural characteristics. There is no obvious reflector within the upper crust of the eastern segment of the Helan Mountains (i.e., Profile Distance 45–56 km). These phenomena indicate that the stratum lithology and structure of the eastern and western segments of the Helan Mountains are different. Based on geological data, the exposed granitic pluton is east of Profile Distance ~50 km, and a Mesozoic-Paleozoic sedimentary rock layer is on the western side (Figure 4a). Within the Yinchuan Basin, east of Profile Distance ~56 km, multiple groups of reflection events from Cenozoic sedimentary strata have strong reflection energies and good lateral continuity. According to the longitudinal and lateral distribution characteristics of reflections from these sedimentary layers, the thickest Cenozoic deposition is under Profile Distance ~90 km and the corresponding thickness of the Cenozoic sedimentary stratum is 7000–7200 m. East of Profile Distance ~110 km, which is the Ordos Platform, basement reflector Tg is gently west-dipping, and the Cenozoic stratum here is found to be obviously thinner, with a deduced thickness of less than 2200 m.

The basement P-wave velocity structure along the profile (Figure 3a) reflects similar structural characteristics as the upper crust in the stacked deep seismic reflection section. In the Alashan block's eastern margin located west of Profile Distance ~23 km, P-wave velocities less than 3500 m s^{-1} are found at depths of ~2400 m or less, and P-wave velocities here were significantly lower than those in the Helan Mountains area, which indicates that a sedimentary layer with a relatively looser structure lies above the basement. The basement velocity structure for the Helan Mountains uplift zone exhibits obvious high-velocity characteristics. The near-surface P-wave velocities of this section are generally 4000–4500 m s^{-1}, reaching 5000 m s^{-1} at some locations. The basement distribution of the Helan Mountains area is steep in the east and gentle in the west, which is consistent with the terrain and topographical features of the Helan Mountains. The Yinchuan Basin is a Cenozoic rifted basin, and its overall P-wave velocities indicate low-velocity structures; this is obviously related to the thicker Cenozoic sedimentary stratum within the basin. With increasing depth, P-wave velocities within the basin soars with a positive gradient, as do the gravitational compaction and the stratum's degree of consolidation. The basement of the Yinchuan Basin appears as a stepped slope zone on the eastern and western sides of the basin. A remarkable change in thickness of the sedimentary cover occurs at the basement jump, indicating that the basement structure and sedimentary stratum thickness are affected and controlled by the fault zone.

4.2 Reflection structure characteristics of the middle-lower crust

The middle-lower crustal structure of this region, bounded laterally by Profile Distance ~65 km, has completely different reflection fields on its eastern and western sides. To the west of Profile Distance ~65 km, the deep seismic reflection profile reveals a series of middle-lower crustal reflections with strong reflection energy, dense reflection phases, and varying lateral continuity lengths. This suggests that the middle–lower crust of the Helan Mountains might contain rock mass units with obvious differences in wave-impedance, non-uniform occurrence scales, and high-and-low velocity distributions, which lead to an abundance of reflection groups and a complex reflection structure in the middle-lower crust of the Helan Mountains. It can be seen from the crustal 2D velocity structure (Figure 3b) that the middle-lower crust of the Helan Mountains is characterized by a high-and-low velocity distribution, and there is an obvious low-velocity layer in the middle-lower crust (i.e., LVL1 and LVL2). The complicated reflection structure and unusual velocity structure of the Helan Mountains' middle-lower crust and the presence of a series of compressed folds in the upper crust all indicate that the crustal structure of the Helan Mountains underwent strong deformation throughout the lengthy processes of its formation, evolution, and uplift. Compared with the complex structure of the

Helan Mountains, the middle-lower crustal reflection energy of the Yinchuan Basin and Ordos block's western margin is significantly weaker, and there is no strong continuous reflector within the middle-lower crusts, with the exception of the sectional continuous reflection phase, CR_2, which is faintly visible at TWT 10–11 s. This indicates that the middle-lower crust of the Yinchuan Basin and Ordos block's western margin has weaker structural deformations and it probably consists of completely different crustal material compared to the Helan Mountains.

The middle-lower crust beneath the Helan Mountains has complex reflection structures and disorderly reflection phases. Close observation of the attitudes of the reflection events and density variations of reflection phases reveals that the middle-lower crust of the Helan Mountains displays different distributional characteristics of reflection events in the upper and lower regions when it is bounded by the CR_2 reflection interface. In the middle crust between the CR_1-CR_2 interfaces, the reflection events are mostly east-dipping monoclinic structures. However, in the lower crust beneath the CR_2 reflection interface, profile reflections are dominated by the west-dipping or nearly horizontal reflection events, with the intermittent appearance of crisscrossing and merging. The two completely different sets of reflection structures above and below the CR_2 interface might indicate that this interface is the decoupling plane for structural deformation of the middle and lower crust, and is also the main evidence determining the boundary between the middle and lower crusts.

4.3 Reflection structure characteristics of the Moho and lithospheric mantle

The deep seismic reflection profile reveals that the Moho reflection waves have strong reflection energy and good lateral continuity. However, the Moho reflection waves from different profile locations have varying characteristics. In the Yinchuan Basin and Ordos block's western margin, the Moho reflection has a strong phase reflection zone with a duration of approximately TWT 0.5–0.7 s (1.6–2.2 km thick). Underneath the Helan Mountains, the Moho reflection and a series of strong reflections from the lower crust overlap and become indistinguishable. These characteristics point to possible differences between the crustal bottom material structure and media properties of the Yinchuan Basin and Ordos block's western edge and those of the Helan Mountains.

The crust-mantle boundary is characterized by significant diminishing or disappearance of the Moho's strong reflection energy, and thus the crustal thickness and undulating Moho morphology vary along the profile. Underneath the Ordos block's western margin and the Yinchuan Basin, the Moho interface is shown as a monoclinic form plunging from west to east. The shallowest Moho interface with a depth of 39–40 km is located in the Yinchuan Basin, while the depth is 42–43 km beneath the Ordos block at the eastern end of the profile. The Moho interface becomes noticeably deeper in the Helan Mountains and the Alashan block's eastern margin and is deepest (~48 km) beneath the Helan Mountains along this profile.

From the staked deep seismic reflection time section, we can see that the deepest interface reflection is the UMR. The two-way travel time of this strong reflection is approximately 22.0–24.0 s, with a corresponding interface at a depth of 82–92 km. In light of the distributional characteristics of the UMR on the profile, the depth of the UMR is shallow underneath the Helan Mountains and west of the Yinchuan Basin, and gradually deepens toward the profiles' eastern and western sides. The appearance of a strong UMR indicates a physical interface with a wave impedance difference or a velocity jump layer in the upper mantle of the study region.

5. Faulting characteristics of deep seismic reflection profile

The 135-km-long deep seismic reflection profile reveals a series of faults formed during different geological periods, and they have varying tectonic characteristics bounded by the Helan Mountains. Within the Yinchuan Basin, both the eastern piedmont fault of the Helan Mountains (F_3) and the Luhuatai fault (F_4) are east-dipping normal faults. The basement to the west of Yinchuan Basin is a stepped slope that gradually deepens from west to east, but the depth of the basement appears to change suddenly beneath faults F_3 and F_4. The Yinchuan fault (F_5) and Yellow River fault (F_6) on the profile are west-dipping normal faults, and they are located near Profile Distances 96 and 110 km, respectively. These two faults control the sedimentary structure and the basement distribution to the east of the Yinchuan Basin. The thickest sedimentary layer (7000–7200 m) is located on the down-dropped block of the Yinchuan fault. On the whole, the thickness of the Cenozoic sedimentary layer and basement structure in the Yinchuan Basin are mainly controlled by the eastern piedmont fault of the Helan Mountains, the Luhuatai fault, the Yinchuan fault, and the Yellow River fault. The alternating activities of these faults form a graben-within-graben basin structure. Meanwhile, these faults also form a "negative flower" fault structure that extends to the middle–lower crust and the top of the upper mantle, belonging to the crustal-scale deep fault system. From analyses of the substantial arching and deformation of the CR_1 interface near the deep faults and the extrusion folds near the faults, we infer that the deep faults experience a certain amount of thrusting motion concurrently with the strike-slip motion. The series of upper crustal Cenozoic normal faults within the Yinchuan Basin might have been the result of the Mesozoic (or earlier) thrusting strike-slip

faults. The current, younger extensional faults were subsequently superimposed on the terrane that had been jointly acted upon by thrusting and strike-slip tectonics.

Based on the geological data of the study area, the main outcrops in the Helan Mountains include Paleozoic-Mesozoic sedimentary sandstone, Archean crystalline basement, and a series of intrusive rocks. There is an unconformity where the Cenozoic sedimentary layer overlaid the pre-Cenozoic stratum (Ningxia Hui Autonomous Region Geological Bureau, 1990). Studies by Liu et al. (2010) showed that a series of east-dipping Mesozoic-Paleozoic thrust faults developed in the Helan Mountains uplift zone. Our deep seismic reflection profile further indicates the presence of various west-dipping Mesozoic-Paleozoic stratum folds with strong reflection energy distributed intermittently in the western Helan Mountains. In view of the structure of the reflection waves and their distributional pattern along the profile, these stratum folds are mainly controlled by three east-dipping and spade-shaped thrust faults, i.e., the Bayanhaote fault (F_1), the western piedmont fault of the Helan Mountains (F_2), and the buried thrust fault ($F_{1\text{-}1}$). At depths shallower than ~15 km, these three thrust faults cause folding and thrusting of the Mesozoic–Paleozoic stratum in the western Helan Mountains, and the deep layers then jointly form an overthrust nappe structure with the upper crustal bottom interface at a depth of ~18–20 km, which in turn results in folding, uplifting, and structural deformation of the stratum within the nappe structure's hanging wall. The crustal 2D velocity structure (Figure 3b) indicates the presence of obvious low-velocity structures within the middle crust beneath the CR_1 interface of the Helan Mountains, which suggests that an obvious velocity discontinuity exists at corresponding depths. The velocity is 6.38 km s^{-1} above the discontinuity interface, under which it is 6.30 km s^{-1}. The overthrust nappe structure shown by the deep seismic reflection profiling is located at the bottom of the upper crust. Affected by regional tectonic stress, the middle crustal low-velocity layer facilitated the lateral sliding of the upper crustal nappe structure.

6. Results and discussion

The HM-YB is both a tectonic deformation zone and an active tectonic zone of the western NCC. Our deep seismic reflection profiling analysis clearly revealed the deep fine structure, fault tectonic patterns, and structural differences between this tectonic zone and adjacent blocks. By integrating the basement velocity distribution along the profile, reflection structural images of the crust and upper mantle, crustal P-wave velocity structure, and geological data of the study area, we constructed a comprehensive interpretation of the deep seismic reflection profile (Figure 5). Analyses and detailed discussions of the results are as follows.

(1) The crustal structure is distinctly different between the HM-YB and its adjacent blocks. The crust of the study area has a clear three-layers structure (i.e., the upper crust, middle crust, and lower crust), and the crustal thickness, crustal reflection structure imaging, and intra-crustal P-wave velocity distributions are significantly different among various tectonic sections along the profile. The crustal thickness of the Yinchuan Basin and the Ordos block's western margin

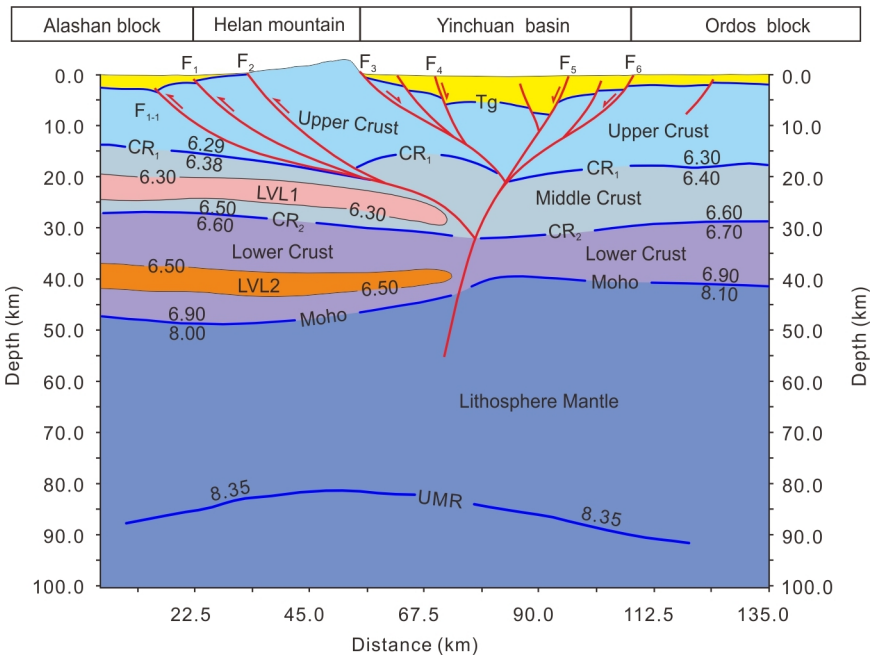

Figure 5 Interpretation of the deep seismic reflection profile. Blue line marks subsurface interface; red line indicates fault; numerals are P-wave velocities obtained from the wide-angle reflection/refraction profile; fault number is the same as in Figures 1 and 4.

changes in the range from 40 to 42 km, with the intra-crustal P-wave velocity increasing with depth in a positive gradient. There is a Moho uplift of 2–3 km beneath the Yinchuan Basin, corresponding to a mirror image of the basin basement. The area beneath the Helan Mountains is the thickest part of the crust along the profile, with a corresponding crustal thickness of 48 km. In addition, an interbedded structure with distinct high-low velocities exists within the middle-lower crust of the Helan Mountains. These observations, including the abrupt change in Moho depth on the eastern side of the Helan Mountains, and intra-crustal P-wave velocity distribution between the Helan Mountains and the Yinchuan Basin, indicate that the eastern side of the Helan Mountains is the mutation zone of crustal thickness and the boundary zone of velocity changes.

(2) The deep-shallow tectonic pattern in the Helan Mountains-Yinchuan Basin region is complex. The deep seismic reflection profile demonstrates that the fault structure has significantly different characteristics between the eastern and western sides of the Helan Mountains. On the western side of the Helan Mountains, the Bayanhaote fault (F_1), the western piedmont fault of the HM (F_2), and the buried fault ($F_{1\text{-}1}$) are all east-dipping, "spade-shaped" thrust faults. These faults play an important role in the upper crust structural deformation of the Helan Mountains uplift zone, formation and development of stratum folds, and folding uplift of the Helan Mountains during the Mesozoic-Paleozoic eras. On the eastern side of the Helan Mountains, the Cenozoic Yinchuan Basin is controlled by the eastern piedmont fault of the Helan Mountains (F_3), Luhuatai fault (F_4), Yinchuan fault (F_5), and Yellow River fault (F_6). The alternating activities of these faults have led to the formation of a graben-within-graben basin structure, whose depocenter is located between the Luhuatai fault and Yinchuan fault. At a depth of 18–20 km, a series of Cenozoic normal faults form a "negative flower" fault structure that extends downward to cut the middle-lower crust, and then jointly forms a complex fault tectonic zone with deep crustal faults. This complex tectonic system with varying deep-shallow structural characteristics, formed over different eras, played a pivotal role in controlling the region's basin-mountain coupling and crust-mantle structural deformation.

(3) The crustal reflection structure images of the HM-YB are markedly different from those of adjacent blocks. Crustal reflection structure is closely related to intra-crustal velocity distributions and variations in media properties. Reflection images of a seismic profile can actually more thoroughly reflect the occurrence state of the subsurface interface and the physical differences in the subsurface structure. Hence, application of the deep seismic reflection method can facilitate high-resolution imaging of those structural (or tectonic) layers with obvious differences in wave impedance. The Cenozoic sedimentary layer in the Yinchuan Basin appears as a stratified structure with strong reflection energy. In the upper crust of the Helan Mountains, except for the Mesozoic-Paleozoic sedimentary layer and extrusion folds showing relatively stronger reflection seismic responses, all sections demonstrate disorderly and weak reflections, which may represent Archean crystalline metamorphic rocks or granitic intrusions. In the Helan Mountains' uplift zone, the complex middle-lower crustal reflection structure, thicker crust-mantle transitional zone, and high-low interbedded velocity structure are in contrast to those of the Ordos block, which has a simple middle-lower crustal reflection structure, clear Moho reflection, and depth-dependent velocity distribution with a positive gradient. These phenomena indicate that the Helan Mountain's crustal structure has undergone intense changes over its long period of formation, evolution, and uplift. In contrast, the Ordos block is a stable crustal structure with mild deformation. Based on the profile's reflection structural images and crustal velocity structure distribution, we believe that the crustal deep fault is the deep tectonic boundary between the tectonic deformation zone of the HM-YB and the stable Ordos block, while the shallow tectonic boundary is the Yellow River fault.

(4) The UMR shown in the deep seismic reflection section greatly contributed to our understanding of the region's longitudinal inhomogeneity in the upper mantle structure and the deep dynamic processes. The depth of the UMR is 82–92 km. Beneath the HM-YB, the UMR uplifts significantly, while the eastern and western sides plunge to the Ordos and Alashan blocks, respectively. The depth of the UMR measured in this study is essentially consistent with that of the upper mantle L1 interface on the Wendeng-Alashan Left Banner wide-angle reflection/refraction profile (Wang et al., 2014), as well as that of the upper mantle reflection (R_{U3}) in the Hetao Basin deep seismic reflection profile (Feng et al., 2015). This indicates that a strong reflection interface may be prevalent at 80–100 km depth within the Yinchuan-Hetao rift zone. Chen et al. (2014) found an intralithospheric discontinuity with negative polarity in a low-velocity structure at a depth of 80–100 km beneath the NCC's central and western region, and believed that the ILD might be an ancient and mechanistically weak zone within the lithospheric mantle. Recent studies on lithospheric thicknesses within the NCC reckoned that the lithospheric thickness in its central-western region exhibits strong lateral inhomogeneity, i.e., the lithospheric thickness under the Ordos Basin is ~200 km, whereas under the Yinchuan-Hetao and Shaanxi-Shanxi rift zones, it is less than 100 km, and its lateral variation is larger. (Chen et al., 2009, 2010; Zhu et al., 2011; Yang et al., 2013). Limited by the short length of the deep seismic reflection profile and lack of reflection event data deeper than the UMR in this study, we were unable to determine the seismic wave velocities beneath the UMR. Based solely on results from the deep seismic reflection profile, we could not determine whether the UMR is

from the lithosphere-asthenosphere boundary (LAB) or the weak layer within the lithospheric mantle. Nevertheless, the appearance of strong UMRs provided another piece of evidence for the confirmation of the existence of a velocity discontinuity or transitional layer at 80–100 km depth beneath the western NCC.

In conclusion, the deep seismic reflection profiling revealed various phenomena in the study area including UMR uplifting beneath the HM-YB, a complex fault system cutting the entire crust, distinctly different crustal structure images and intra-crustal velocity distributions between the Helan Mountains and Ordos Block, and uplift of the Moho beneath the Yinchuan Basin. All these characteristics not only jointly contribute to the deep-shallow tectonic background of the study area, but also provide the deep structural conditions for deep substance migration, structural deformation of the crust, and the formation and development of the HM-YB.

Acknowledgements *We thank the leaders and experts at the National Natural Science Foundation of China and North China Craton Major Research Program for their support and assistance during the course of this project. We also thank the Seismological Bureaus of the Ningxia Hui and Inner Mongolia Autonomous Regions, and the Sinopec Geophysical Corporation (North China branch) for their invaluable support during our fieldwork. The probe data were the outcome of the hard work and labor put in by more than 80 staff members of the Geophysical Exploration Center, China Earthquake Administration. We also received guidance and help from academician Zhang Peizhen and researcher Zhang Xiankang in carrying out data processing and interpretation. The chief editor and three reviewers of this journal provided constructive suggestions that improved the final version of this paper. This work was supported by the National Natural Science Foundation of China (Grant No. 91214205) and the Special Scientific Research of Seismological Industry (Grant No. 201408023).*

References

Carlson R W, Pearson D G, James D E. 2005. Physical, chemical, and chronological characteristics of continental mantle. Rev Geophys, 43: RG1001

Chai C Z, Meng G K, Ma G R, Liu B J, Liao Y H, Du P, Wang Y, Lei Q Y, Song F M, Zhao W M, Zhang J H, Xie X F, Sheng J Q. 2011. Active Fault Exploration and Earthquake Hazard Assessment in Yinchuan City (in Chinese). Beijing: Science Press

Chen L, Tao W, Zhao L, Zheng T Y. 2008. Distinct lateral variation of lithospheric thickness in the Northeastern North China Craton. Earth Planet Sci Lett, 267: 56–68

Chen L, Cheng C, Wei Z G. 2009. Seismic evidence for significant lateral variations in lithospheric thickness beneath the central and western North China Craton. Earth Planet Sci Lett, 286: 171–183

Chen L, Wei Z G, Cheng C. 2010. Significant structural variations in the Central and Western North China Craton and its implications for the craton destruction (in Chinese). Earth Sci Front, 17: 212–228

Chen L, Jiang M, Yang J H, Wei Z G, Liu C Z, Ling Y. 2014. Presence of an intralithospheric discontinuity in the central and western North China Craton: Implications for destruction of the craton. Geology, 42: 223–226

Darby B J, Ritts B D. 2002. Mesozoic contractional deformation in the middle of the Asian tectonic collage: The intraplate Western Ordos fold-thrust belt, China. Earth Planet Sci Lett, 205: 13–24

Deng J F, Xiao Q H, Qiu R Z, Liu C, Zhao G C, Yu B S, Zhou S, Zhong C T, Wu Z X. 2006. Cenozoic lithospheric extension and thinning of North China: Mechanism and process (in Chinese). Geol China, 33: 751–761

Deng Q D, Cheng S P, Min W, Yang G Z, Ren D W. 1999. Discussion on Cenozoic tectonics and dynamics of Ordos block. J Geomechanics, 5: 13–21

Duan Y H, Liu B J, Zhao J R, Liu B F, Zhang C K, Pan S Z, Lin J Y, Guo W B. 2015. 2-D P-wave velocity structure of lithosphere in the North China tectonic zone: Constraints from the Yancheng-Baotou deep seismic profile. Sci China Earth Sci, 58: 1577–1591

Feng S Y, Liu B J, Ji J F, He Y J, Tan Y L, Li Y Q. 2015. The survey on fine lithospheric structure beneath Hohhot-Baotou Basin by deep seismic reflection profile (in Chinese). Chin J Geophys, 58: 1158–1168

The research group of active fault system around Ordos Massif, SSB. 1988. Active Fault System Around Ordos Massif (in Chinese). Beijing: Seismological Press

Guo Z, Tang Y C, Chen Y S, Ning J Y, Feng Y G Yue H. 2012. A study on crustal and upper mantle structures in east part of North China Craton using receiver functions (in Chinese). Chin J Geophys, 55: 3591–3600

Lei Q Y, Chai C Z, Zheng W J, Du P, Xie X F, Wang Y, Cui J, Meng G K. 2014. Activity and slip rate of the northern section of yellow river fault revealed by drilling (in Chinese). Seismol Geol, 36: 464–477

Li S L, Lai X L, Liu B F, Wang Z S, He J Y, Sun Y. 2011. Differences in lithospheric structures between two sides of Taihang Mountain obtained from the Zhucheng-Yichuan deep seismic sounding profile. Sci China Earth Sci, 54: 871–880

Liu J H, Zhang P Z, Zheng D W, Wan J L, Wang W T, Du P, Lei Q Y. 2010. Pattern and timing of late Cenozoic rapid exhumation and uplift of the Helan Mountain, China. Sci China Earth Sci, 53: 345–355

Liu Z, Wang F Y, Zhang X K, Duan Y H, Yang Z X, Lin J Y. 2015. Seismic structure of the lithosphere beneath eastern North China craton: Results from long distance deep seismic sounding (in Chinese). Chin J Geophys, 58: 1145–1157

Ningxia Hui Autonomous Region Geological Bureau. 1990. Regional Geology of Ningxia Hui Autonomous Region (in Chinese). Beijing: Geological Publishing House

Ren J Y, Tamaki K, Li S T, Zhang J X. 2002. Late Mesozoic and Cenozoic rifting and its dynamic setting in Eastern China and adjacent areas. Tectonophysics, 344: 175–205

Sheriff R E, Gardner L W. 1999. Exploration Seismology (in Chinese). Beijing: Petroleum Industry Press

Tang X Y, Guo Z M, Chen H L. 1992. The Study and Petroleum Prospecting of Thrust Nappe in the West Margin of Shanxi-Gansu-Ningxia Basin (in Chinese). Xi'an: Northwest University Press

Tian Y, Zhao D P, Sun R M, Teng J W. 2009. Seismic imaging of the crust and upper mantle beneath the North China Craton. Phys Earth Planet Inter, 172: 169–182

Wang S J, Wang F Y, Zhang J S, Jia S X, Zhang C K, Zhao J R, Liu B F. 2014. The P-wave velocity structure of the lithosphere of the North China Craton—Results from the Wendeng-Alxa Left Banner deep seismic sounding profile. Sci China Earth Sci, 57: 2053–2063

Wu F Y, Xu Y G, Zhu R X, Zhang G W. 2014. Thinning and destruction of the cratonic lithosphere: A global perspective. Sci China Earth Sci, 57: 2878–2890

Xu X W, Ma X Y, Deng Q D. 1993. Neotectonic activity along the Shanxi rift system, China. Tectonophysics, 219: 305–325

Xu Y G. 2007. Diachronous lithospheric thinning of the North China Craton and formation of the Daxin'anling-Taihangshan gravity lineament. Lithos, 96: 281–298

Yan L H, Wang L. 2002. Geothermal system in the Yinchuan Basin (in Chinese). Yinchuan: Ningxia People's Press

Yang S, Xiong X, Zheng Y, Shan B. 2013. Upper-mantle temperature and lithospheric thickness of North China (in Chinese). Chin J Geophys, 56: 3855–3867

Yilmaz O. 1994. Seismic Data Processing (in Chinese). Beijing: Petroleum

Industry Press
Zhang J, Toksöz M N. 1998. Nonlinear refraction traveltime tomography. Geophysics, 63: 1726–1737
Zhang J S, He Z X, Fei A Q, Li T B, Huang X N. 2008. Epicontinental mega thrust and nappe system at north segment of the western rim of the Ordos block (in Chinese). Chin J Geol, 43: 251–281
Zhang H S, Tian X B, Liu F, Cao J Q, Teng J W. 2009. Structure of crust and mantle beneath the Hubao Basin and its adjacent region (in Chinese). Progr Geophys, 24: 1609–1615
Zhang Y Q, Mercier J L, Vergély P. 1998. Extension in the graben systems around the Ordos (China), and its contribution to the extrusion tectonics of south China with respect to Gobi-Mongolia. Tectonophysics, 285: 41–75
Zhang Y Q, Ma Y S, Yang N, Shi W, Dong S W. 2003. Cenozoic extensional stress evolution in North China. J Geodyn, 36: 591–613
Zhao H G, Liu C Y, Wang F, Wang J Q, Li Q, Yao Y M. 2007. Uplift and evolution of Helan Mountain. Sci China Ser D-Earth Sci, 50: 217–226
Zheng Y F, Wu F Y. 2009. Growth and reworking of cratonic lithosphere. Chin Sci Bull, 54: 3347–3353
Zhu G, Hu Z Q, Chen Y, Niu M L, Xie C L. 2008. Evolution of early cretaceous extensional basins in the eastern North China Craton and its implication for the craton destruction (in Chinese). Geol Bull China, 27: 1594–1604
Zhu R X, Chen L, Wu F Y, Liu J L. 2011. Timing, scale and mechanism of the destruction of the North China Craton. Sci China Earth Sci, 54: 789–797
Zhu R X, Xu Y G, Zhu G, Zhang H F, Xia Q K, Zheng T Y. 2012. Destruction of the North China Craton. Sci China Earth Sci, 55: 1565–1587